JOURNAL OF MATERIALS SCIENCE **36** (2001) 1093–1098

Oxide-ion conducting ceramics for solid oxide fuel cells

K. HUANG, J. WAN, J. B. GOODENOUGH
Texas Materials Institute, ETC 9.102, The University of Texas at Austin, TX 78712-1063, USA
E-mail: jgoodenough@mail.utexas.edu

Realization of a solid oxide fuel cell (SOFC) operating at 700°C on a hydrocarbon fuel or gaseous H_2 is an outstanding technical target. For the past 25 years, efforts to achieve this goal have been based on yttria-stabilized zirconia as the electrolyte, a NiO + electrolyte composite as the anode, a porous $La_{0.85}Sr_{0.15}MnO_3$ (LSM) metallic perovskite as the cathode, and a $La_{1-x}Sr_xCrO_3$ ceramic as the interconnect material. This paper reviews progress in our laboratory on an alternate approach that would use a Sr- and Mg- doped $LaGaO_3$ perovskite as the electrolyte, a Sm-doped ceria (SDC) as the anode or as a buffer layer with a NiO + SDC composite as the anode, a mixed oxide-ion/electronic conductor (MIEC) as the cathode, and a stainless steel as the metallic interconnect.

1. Introduction

Ceramic membranes for the conversion of fossil fuel to electric power or to higher-value products as well as those for gas separation, gas sensing, and removal of noxious pollutants such as NO_x, SO_x, H_2S and unburned hydrocarbons all rely on oxide-ion conductors, either electrolytes or mixed oxide-ion/electronic conductors (MIECs). This paper focuses on one principal target: A solid oxide fuel cell (SOFC) operating at 700°C with either H_2 or hydrocarbon fuels.

The U. S. Department of Energy has made a massive commitment over the past 25 years to the development of a SOFC based on yttria-stabilized zirconia (YSZ) as the solid electrolyte. Thin-film YSZ-based SOFCs have achieved high power density at 800°C, but the power density decreases quickly with decreasing temperature. The high $La_{0.85}Sr_{0.15}MnO_3$ (LSM) cathode overpotential at low temperature is the primary reason for the power loss. To obtain a SOFC operating at or below 700°C, there is a clear need to begin with a different oxide-ion electrolyte that is compatible with catalytically active electrode materials at low temperatures. We begin with the $La_{1-x}Sr_xGa_{1-y}Mg_yO_{3-0.5(x+y)}$ perovskite as the solid electrolyte since it possesses the same structure as good cathode materials. This perovskite system was first identified as a good oxide-ion electrolyte by Ishihara *et al.* [1] and verified in a parallel study [2], but the initial compositions were two-phase. Optimization of a single-phase composition was subsequently accomplished by Huang and Petric [3] and by ourselves [4].

A mixed oxide-ion/electronic conductor (MIEC) is recognized to offer the best solution for the cathode of a SOFC; it may also prove to be the best solution for the anode. Determination of the relative rates of oxide-ion transport across an electrode and catalytic oxidation of the fuel at the anode surface or reduction of O_2 to $2O^{2-}$ at the cathode surface is required to optimize the morphology of the electrodes. Once this determination is made, it is a natural step to inquire how MIEC oxygen-permeation membranes might be fabricated for use in other applications.

2. Experimental procedures

2.1. Sample preparation

The electrolyte composition $La_{0.8}Sr_{0.2}Ga_{0.83}Mg_{0.17}O_{2.815}$ (LSGM) was chosen as our previous study [4] has shown it to be optimal. It was made from solid-state reaction as described in detail in [4]. Sintered pellets more than 99% dense were obtained after a final sintering at 1470°C for 24 hours. The pellets were subsequently ground down to a thickness of about 500-μm for our fuel-cell tests. LSGM samples doped with Ni or Co in place of some of the Mg were fabricated in a similar way; samples with formulae $La_{0.8}Sr_{0.2}Ga_{0.83}Mg_{0.1}Ni_{0.07}O_{3-\delta}$ and $La_{0.8}Sr_{0.2}Ga_{0.83}Mg_{0.1}Co_{0.07}O_{3-\delta}$ are designated LSGMN and LSGMC, respectively. Higher doping led to the presence of impurities.

Both the cathode and the anode materials were synthesized by a wet-chemical route. The Pechini process, based on a carboxylate group such as citric acid as the chelating agent, was selected for the synthesis of precursors of all electrode powders except $SrCo_{0.8}Fe_{0.2}O_{3-\delta}$ (SCF). The exact composition of each electrode and their synthesis condition are summarized in Table I. Single-phase SCF proved difficult to make by a normal Pechini process. The hexagonal $SrCoO_2$ that contains no oxygen vacancies was always preferentially formed in addition to the desired perovskite phase. We attributed this behavior to an uneven distribution of Sr^{2+}

TABLE I Electrode preparation conditions

Compositions	Symbol	Synthesis method	Decomposition temperature	Sintering temperature	Phases
$La_{0.6}Sr_{0.4}CoO_{3-\delta}$	LSCo	Pechini	750°C	1250°C	Rhombohedral
$La_{0.8}Sr_{0.2}Co_{0.8}Ni_{0.2}O_{3-\delta}$	LSCN	Pechini	750°C	1300°C	Rhombohedral
$La_{0.7}Sr_{0.3}Fe_{0.8}Ni_{0.2}O_{3-\delta}$	LSFN	Pechini	750°C	1400°C	Rhombohedral
$SrCo_{0.8}Fe_{0.2}O_{3-\delta}$	SCF	EDTA	750°C	1000°C	Primitive Cubic
$La_{0.85}Sr_{0.15}MnO_3$	LSM	Pechini	750°C	1400°C	Orthorhombic
$Ce_{0.8}Sm_{0.2}O_{1.9}$	SDC	Pechni	750°C	1450°C	Fluorite Cubic
$Ce_{0.8}Sm_{0.2}O_{1.9}$ + NiO	SDC + NiO	Pechini	750°C	1400°C	Two cubic phases

in the solution as a result of only partial coordination of some of the Sr^{2+} ions by the relatively weak chelation of the carboxylate ligands of citric acids. Therefore, we choose ethylenediaminetetraacetic acid (EDTA) as the chelating agent since all cations of SCF coordinate strongly with EDTA according to their larger formation constants for chelation. The use of EDTA suppressed the segregation of Sr^{2+} in the Pechni process, and well-crystallized, single-phase cubic SCF powders were obtained at temperatures as low as 1000°C.

The structures of the electrolyte and electrode powders were examined at room temperature by powder x-ray diffraction with a Philips PW1729 diffractometer operating with Cu K_α radiation and Ni filter. To obtain accurate lattice parameters, synthesized silicon powder was used as an internal standard and Rietveld refinement was used to process the raw x-ray data.

2.2. Impedance spectroscopy

Pt was used to evaluate the electrolyte conductivity by two-probe ac-impedance measurement. Pt paste from Heraeus was coated on both ends of the electrolyte pellets, which were baked for a half-hour at 900°C. To study the MIEC cathode resistances with LSGM as the electrolyte, we used a similar procedure. Each cathode powder was first well-mixed with an organic binder from Heraeus to form an ink that was pasted on two ends of an LSGM pellet; the pellet was then fired typically at 1150°C for a half-hour. All measurements were made on cooling from 800°C down to 320°C in air with a HP 4192A LF impedance analyzer in a range of frequency from 5 Hz to 13 MHz with an amplitude of 10 mV. The bulk and overall conductivities of the electrolyte were extracted from the intersections with the real axis of related bulk and grain-boundary semicircles in the impedance spectra. The individual electrode resistances were calculated from the real part of the impedance at the lowest frequency 5 Hz to the first intersections with the real axis. The lead resistance was subtracted out from all data by measuring the resistance of a blank cell.

2.3. Single fuel-cell tests

To avoid a possible reaction of Ni in the anode with the LSGM electrolyte, we used $Ce_{0.8}Sm_{0.2}O_{1.9}$ (SDC) as a thin buffer layer between LSGM and a composite SDC + NiO anode; the NiO is reduced in the anode atmosphere to form a porous SDC anode with elemental nickel particles on the inside of the pores. The anode and the SDC buffer layer were fabricated on one side of a 500-μm-thick electrolyte disk ~18 mm in diameter by screen-printing a slurry of the anode ink and baking at 1300°C in air for a half-hour. A Pt mesh with a Pt lead was used as the current collector. The cathode ink was then screen-printed on the opposite surface with a Pt current collector placed on it; the assembly was baked in air at 1150°C for 2 hours. The effective electrode area was 0.24 cm^2. Reference electrodes of the same materials as the working electrodes were used to monitor the overpotentials of the cathode and anode in the cell configuration of Fig. 1. As described in an earlier

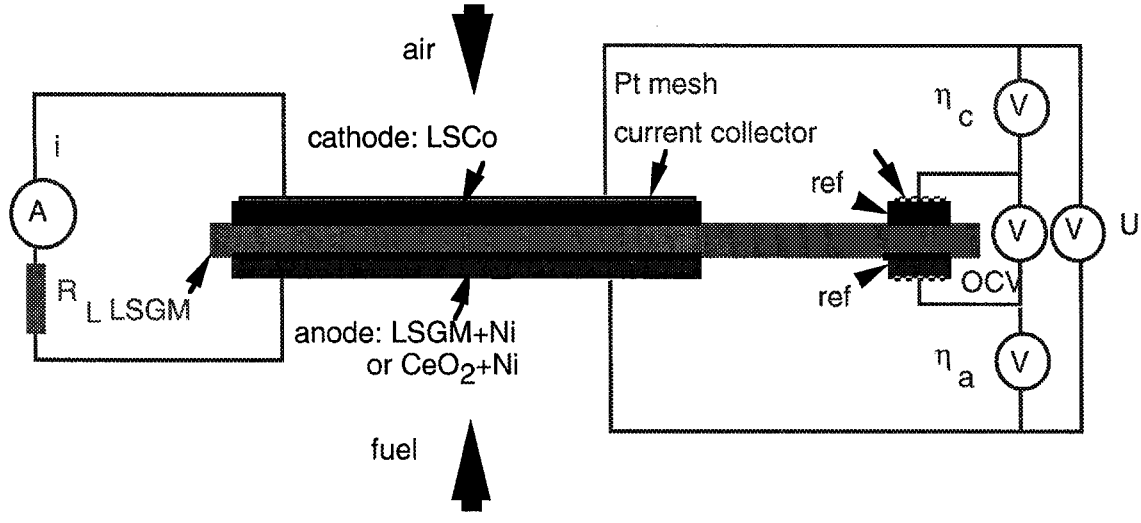

Figure 1 Single solid oxide fuel cell configuration.

study [5, 6], we measured the voltage output of the cell as well as the electrode overpotentials versus current density with H_2 as the fuel and air as the oxidant. The cells were glass-sealed into Al_2O_3 tubes *in situ* with a special glass developed in our laboratory.

The test cells were placed in the hot zone of a vertical furnace. Air was supplied directly to the cathode surface; water-moistened (at ∼30°C) hydrogen was fed to the anode surface at a rate of 40–60 ml/min. All of the tests were performed with an EG&G Potentiostat/Galvanostat Model 273 running on a homemade LabView program; they are carried out in the temperature range $600°C < T < 800°C$ with an interval of 50°C. With the four-electrode configuration of Fig. 1, typical V-I measurements were taken at a fixed temperature from open-circuit voltage (OCV) to 0.4 V and back to OCV in steps of 20 mV and holding 10 seconds at each point.

3. Results and discussion

3.1. The electrolyte

Fig. 2, shows the oxide-ion conductivity of the LSGM is $\sigma_o \approx 0.15$ S/cm at 800°C, which is equivalent to YSZ at 1000°C; the break in $\ln \sigma_o T$ vs. $1/T$ at $T^* \approx 590°C$ signals the nucleation of clusters of ordered oxide-ion vacancies and a progressive condensation of the mobile vacancies into these clusters with decreasing temperature [4]. Fig. 2 also shows that partial substitution of Ni or Co for Mg in LSGM increases the total low-temperature conductivity; it appears to suppress the formation of clusters of ordered oxide-ion vacancies, but it also introduces an electronic component at low temperatures. The Mg^{2+} ions have a greater tetragonal-site stability and therefore a stronger attraction for the vacancies they introduce. Although Ni and Co substitutions introduce some electronic conductivity, the oxide-ion transport number $t_o = \sigma_o/\sigma$ is not significantly reduced at 700°C by substitution of 7 mol% Ni on Ga sites as can be seen by the LSGMN curve of Fig. 3 compared to Co-doping; the Co(II) ion is more easily oxidized than Ni(II). These values of t_o were obtained by comparing the open-circuit voltage (OCV) across the electrolyte with the theoretical value for a given difference in the partial pressure of oxygen on either side: $t_o \equiv (\text{OCV})_{\text{meas.}}/(\text{OCV})_{\text{theory}}$. It is noticed that the OCV increases with decreasing temperature provided that the electronic conduction in the electrolyte is negligible as in the case of LSGM. On the other hand, if the electronic conduction becomes appreciable as shown in the case of LSGMN and LSGMC, the cell OCV would decrease with decreasing temperature.

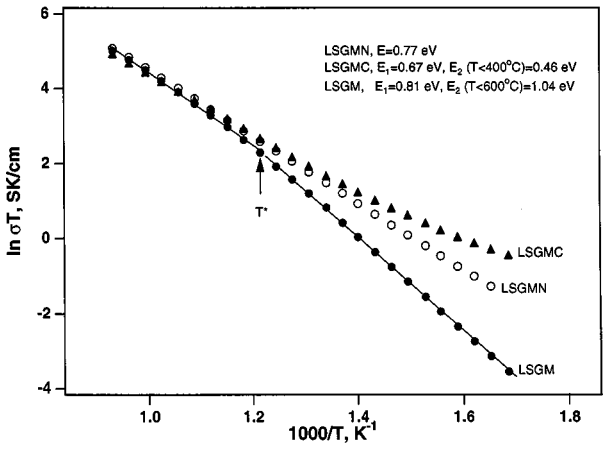

Figure 2 Conductivity comparison of LSGM, LSGMN and LSGMC.

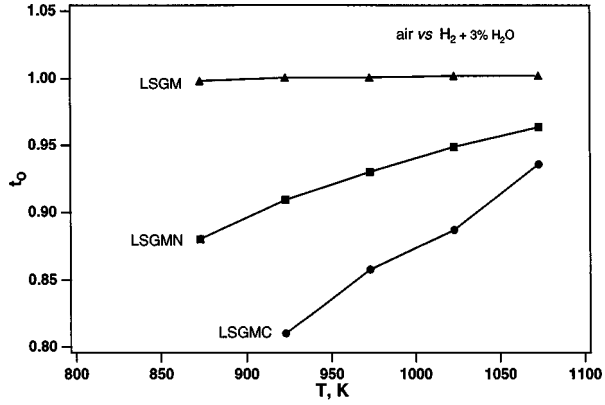

Figure 3 Oxide-ion transport numbers of LSGM, LSGMN and LSGMC as a function of temperature.

The data of Fig. 3 imply that interdiffusion of Ni or Co (and probably Fe also) across an LSGM/cathode interface does not produce blocking phases at the interface that are harmful to oxide-ion conduction across it. We [7] have monitored an interdiffusion of Co and Ga across an LSGM/$La_{1-x}Sr_xCoO_{3-\delta}$ interface and found that the interdiffusion improves the contact so as to enhance O^{2-} ion diffusion across the interface; it does not degrade performance. Therefore, we are confident that we can use an MIEC cathode containing Fe, Co, and/or Ni in conjunction with the LSGM electrolyte without forming blocking phases at the interface.

On the anode side, we have demonstrated that LSGM does not react with SDC at moderate temperature. The SDC becomes an MIEC in the reducing atmosphere at the anode. An LSGM-based single cell with a Ni-free SDC anode is under investigation in our laboratory.

3.2. The electrodes

In order to avoid restriction of the catalytic reaction to a three-phase line interface, it would be advantageous to have as an electrode an MIEC that is intrinsically active in the catalytic deep oxidation of the fuel at the anode and the reduction of gaseous O_2 to $2O^{2-}$ at the cathode. Minimization of the electrode overpotentials is critical, particularly for reduced-temperature applications.

The SOFC anode. In our preliminary studies [5, 6], we used as our anode NiO + SDC composite on top of a thin SDC buffer layer. The maximum power density has been increased more than 100 mW/cm^2 compared to a cell without an SDC buffer layer. We believe the SDC layer prevents a possible reaction between NiO and LSGM and enhances the catalytic reaction at the anode surface. Recently, Park *et al.* [8] have pointed out that SDC can also deeply oxidize hydrocarbons to CO_2 and H_2O whereas carborization occurs at a nickel catalyst. They made a composite SDC and Cu to improve

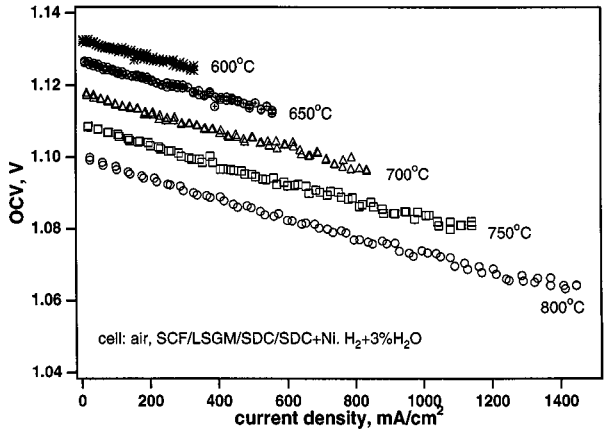

Figure 4 Dependence on current density of the open-circuit voltage at various temperatures.

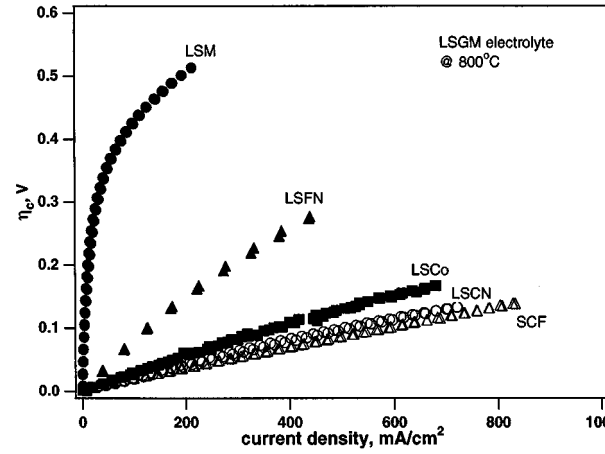

Figure 5 Cathode overpotentials of different cathode materials as a function of current density at 800°C.

the electronic conductivity of the anode; but Ce^{4+} is partially reduced to Ce^{3+} to make SDC an MIEC in the reducing atmosphere at the anode. Optimization of the morphology of an SDC or SDC + Cu anode would balance the rate of fuel oxidation and current collection at the surface with the rate of O^{2-} ion transport across an SDC film.

With an H_2 flow rate of 40 to 60 ml/min, the OCV versus current density I of Fig. 4 was obtained by monitoring the voltage across the two reference electrodes of Fig. 1 while current was flowing across the working electrodes. The fuel utilization was estimated to be high at all flow rates. The decrease in the OCV with increasing current density is believed to be due to the generation of water in the pores of the anode. If the water is not removed rapidly enough, the cell OCV will be decreased as a result of an increased effective partial pressure of oxygen at the anode. This problem would be eliminated if a dense Ni-free SDC anode were used instead of a porous composite.

The SOFC cathode. Conventional practice with a YSZ electrolyte has been to use LSM as the cathode because it remains a metallic conductor in an O_2 atmosphere. However, LSM is not an oxide-ion conductor in an O_2 atmosphere, so it must be fabricated as a porous structure through which O_2 can penetrate to the electrolyte. This approach has encountered two difficulties: (1) maintenance of the porous morphology over a prolonged period at the operating temperature of the SOFC and (2) chemical reaction between YSZ and LSM at fabrication temperatures to form the pyrochlore $La_2Zr_2O_7$ and the perovskite $SrZrO_3$, neither of which conduct either electrons or oxide ions. We have used the MIEC $La_{1-x}Sr_xCoO_{3-\delta}$ in our preliminary test cells [5], but this material has a larger thermal expansion coefficient (TEC) than LSGM as a result of a low-spin to intermediate-spin transition that occurs at Co(III) ions [9]. Therefore, we have investigated the cathode overpotentials $\eta_c(I)$ for several other cathode materials on an LSGM electrolyte as a function of current density I, Fig. 5, with the test-cell configuration of Fig. 1. The perovskite LSM is clearly the poorest cathode material; The cobalt-containing perovskites SCF, LSCN and LSCo give the best performances, but the TEC remains higher than that of LSGM even with dilution of the cobalt content. The LSFN perovskite has a TEC well matched to that of LSGM. Its performance as a cathode proved better than that of LSM, but it is still not satisfactory in our preliminary tests. From ac impedance spectroscopy, Fig. 6, the electrode resistances are seen to increase in the order SCF < LSCN < LSCo < LSFN < LSM. We have determined with permeation studies [10] that the catalytic activity for the reduction of O_2 to $2O^{2-}$ is responsible for the relative magnitudes of the electrode resistances.

In these studies, we have chosen perovskites that remain metallic in the oxidizing atmosphere at the cathode. In order to retain a mixed oxide-ion/electronic conductivity in an O_2 atmosphere, we use the M(IV)/M(III) redox couples of M = Fe, Co, or Ni as these couples are all pinned at the top of the O-2p band; the degree of M-O covalent mixing in the antibonding σ^* conduction band increases on going from Fe to Co to Ni, but the redox couples all overlap in energy. This situation allows use of two different Fe, Co, or Ni cations without destroying the good electronic conductivity; in an O_2 atmosphere, the Fermi

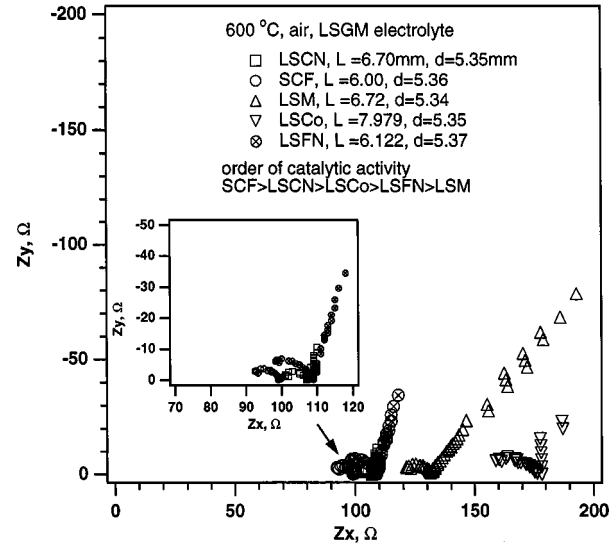

Figure 6 Impedance spectra of LSGM electrolyte with various electrode materials at 600°C.

energy ε_f lies in the σ^* band of the M(IV)/M(III) couples. However, the Fe(IV)/Fe(III) couple is a high-spin $t^3\sigma^{*1}/t^3e^2$ configuration in which localized e electrons tend to occupy Fe(III) ions whereas the Ni(IV)/Ni(III) couple is a low-spin $t^6\sigma^{*0}/t^6\sigma^{*1}$ configuration in which the electrons of e-orbital parentage remain itinerant. At low temperatures, the Co(IV)/Co(III) couple is a low-spin $t^5\sigma^{*0}/t^6\sigma^{*0}$ configuration; but it becomes an intermediate-spin $t^5\sigma^{*0}/t^5\sigma^{*1}$ configuration at the operating temperature of a SOFC. It is the transition from low-spin to intermediate-spin configuration at the Co(III) ions that introduces a higher TEC for the Co-containing perovskites.

The reduction of O_2 to $2O^{2-}$ may occur at an electrode surface by the surface reactions:

$$\text{M(III)-}\square\text{-M(III)} + O_2 = \text{M(IV)-}(O_2)^{2-}\text{-M(IV)}$$

followed by migration of the extra oxygen to another M cation:

$$\text{M(IV)-}(O_2)^{2-}\text{-M(IV)} + \text{M(III)-}\square\text{-M(III)} = 2\text{M(IV)-}O^{2-}\text{-M(IV)}$$

where $\square$ represents an oxygen vacancy. The relative stability of the Fe(III) ion in lower than six oxygen coordination may inhibit these reactions at Fe(III) ions.

3.3. Single-cell performance

Fig. 7 shows the performance from 600 to 800°C of a test cell with a 550-μm thick electrolyte. At 800°C, it is within a factor of two of the best performance obtained with a 10-μm-thick YSZ electrolyte and it still maintains a peak power density of 100 mW/cm^2 at 600°C. The long-term performance is shown in Fig. 8 over a period of 145 hours; the cathode showed no deterioration and the anode showed an initial degradation. The deterioration of the anode is possibly attributed to a coarsening of the Ni catalyst at the operating temperature.

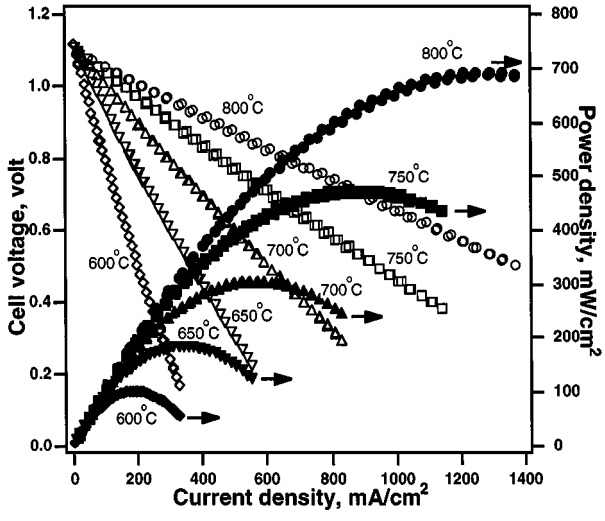

Figure 7 V-I and P-I curves of a single LSGM-based solid oxide fuel cell at various temperatures. The cell consisted of: air, SCF/LSGM/SDC/SDC + Ni, H_2 + 3%H_2O; the LSGM thickness was 550 μm.

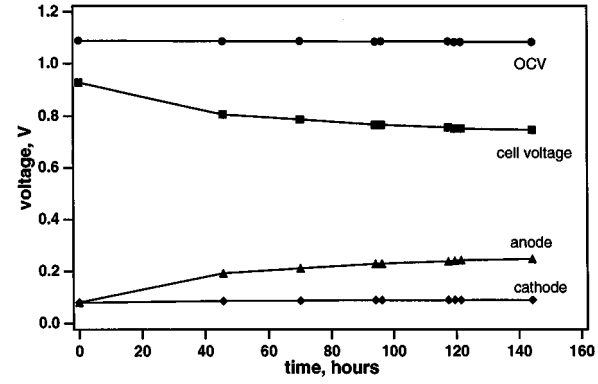

Figure 8 The cathode (a) and anode (b) overpotentials as a function of current density at various temperatures. The cell is the same as shown in Fig. 7.

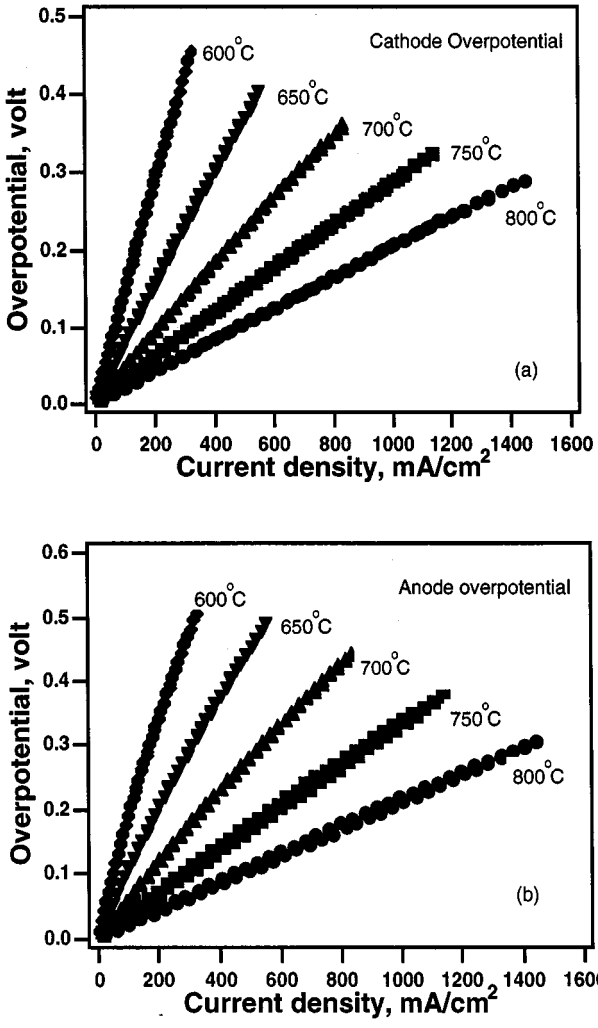

Figure 9 Long-term performance of a single LSGM-based solid oxide fuel cell. The cell is the same as shown in Fig. 7.

It now appears that this problem could be alleviated by using a Ni-free anode such as SDC in our future tests. Fig. 9 shows the anode and cathode overpotentials of the cell against the current density at various temperatures. It is clear that the electrode kinetics would be a rate-determining factor at lower temperatures. Arrhenius plots of the area-specific resistances ASRs for the two electrodes and the total ASR as obtained from

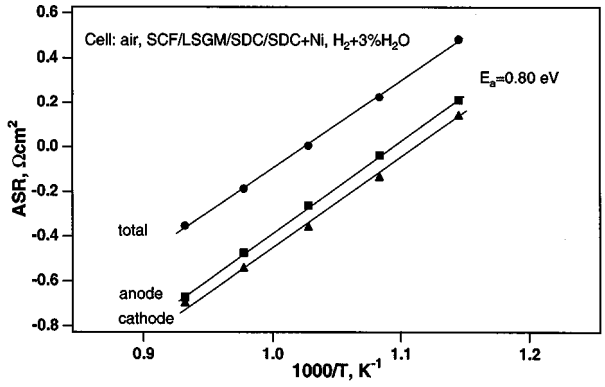

Figure 10 Arrhenius plot of electrode and overall ASRs of the same cell as shown in Fig. 7.

the slopes in Fig. 9 and Fig. 8, respectively, give the same activation energy $E_a = 0.80$ eV, Fig. 10. All these performance data should improve with a thinner electrolyte and optimization of the morphology of the electrodes.

3.4. Fuel-cell stacks

Fabrication of a fuel-cell stack requires identification of a suitable interconnect material. Lowering the operating temperature to below 800°C allows use of an alloy. The principal problem to be solved is the formation of an insulating oxide scale on the air side of the interconnect. A Cr-containing stainless steel produces a Cr_2O_3 scale, and oxidation is particularly rapid where the alloy contacts the MIEC cathode [11]. However, a light coating of Y_2O_3 suppresses growth of the scale beyond a thin film across which electrons can tunnel [12]. Alternate solutions await to be tested. Ceramatec has reported good performance with stacks of four LSGM-based cells fabricated with these materials [13].

4. Conclusions

A set of oxide-ion conducting ceramics has been identified for construction of a SOFC based on LSGM as the solid electrolyte. MIECs can be used for both the anode and the cathode. The morphologies of these electrodes need to be optimized to balance the rate of surface reaction and current collection with the rate of oxide-ion transport across the electrode. Even without this optimization, a maximum power density of 700 mW/cm^2 with a 550-μm-thick LSGM electrolyte has been achieved in a single cell at 800°C with air as the oxidant and $H_2 + 3\%H_2O$ as the fuel. This is the highest performance that has been reported for an LSGM-based cell. The performance data for a single cell and for a four-cell stack indicate that a SOFC based on an LSGM electrolyte can operate below 700°C and would be competitive with a SOFC based on a YSZ electrolyte.

Acknowledgements

MicroCoating Technologies and the Robert A. Welch Foundation, Houston, TX, are thanked for financial support.

References

1. T. ISHIHARA, M. MATRUDA and Y. TAKITA, *J. Am. Chem. Soc.* **116** (1994) 3801.
2. M. FENG and J. B. GOODENOUGH, *Eur. J. Solid State Chem.* **31** (1994) 663.
3. P. HUANG and A. PETRIC, *J. Electrochem. Soc.* **143**(5) (1996) 1644.
4. K. HUANG, R. TICHY and J. B. GOODENOUGH, *J. Amer. Ceram. Soc.* **81** (1998) 2565.
5. K. HUANG, R. TICHY, J. B. GOODENOUGH and C. MILLIKEN, *ibid.* **81** (1998) 2581.
6. K. HUANG, M. FENG and J. B. GOODENOUGH, *J. Electrochem. Soc.* **144** (1997) 3460.
7. *Idem., ibid.* **143** (1996) 3630.
8. S. PARK, J. M. VOHS and R. J. GORTE, *Nature* **404** (2000) 265.
9. K. HUANG, H. Y. LEE and J. B. GOODENOUGH, *J. Electrochem. Soc.* **145** (1998) 3220.
10. K. HUANG, M. SHRÖDER and J. B. GOODENOUGH, in Proceedings of 195th Electrochemical Society Meeting, Seattle, May 1999, edited by E. Wachsman and M. Liu.
11. K. HUANG, P. Y. HOU and J. B. GOODENOUGH, *Solid State Ionics* **129** (2000) 237.
12. *Idem., Mater. Res. Bull.*, accepted.
13. S. ELANGOVAN, J. HARTVIGSEN and A. KHANDAR, in Proceedings of a Joint DOE/EPRI/GRI Workshop on Fuel Cell Technology, San Francisco, May 1998.

Received 5 May
and accepted 25 July 2000